Applied Water Science (2024) 14:62
https://doi.org/10.1007/s13201-024-02116-3

ORIGINAL ARTICLE

Synthesis, characterization of $KAlPO_4F$ and its application for methyl violet adsorption

R. Bagtache[1] · M. Trari[2]

Received: 3 May 2020 / Accepted: 24 January 2024 / Published online: 2 March 2024

Abstract

$KAlPO_4F$ was prepared hydrothermally at 453 K, a time-saving method using cheap reagents. The white solid was characterized by different methods such as powder X-ray diffraction, thermal analysis, SEM and UV–Vis diffuse reflectance. The compound was successfully tested for the removal of methyl violet (MV), a hazardous dye. Experiments were carried out as a function of contact time, initial concentration, temperature and pH. The amount of dye uptake was found to vary with increasing initial solution pH and maximum adsorption was observed at pH 10; the equilibrium was attained in 270 min. The amount of dye uptake (mg/g) was found to increase with increase in dye concentration and contact time. The pseudo-first-order, pseudo-second-order, Elovich and intraparticle diffusion models were applied to fit the experimental data to elucidate the kinetic adsorption. The pseudo-second-order model was the best to describe the adsorption process. Different models analyzed the equilibrium isotherms; the applicability for the experimental data follows the order: Freundlich > Langmuir > Temkin. The thermodynamic parameters: $\Delta H°$ (39.034 kJ mol^{-1}), $\Delta S°$ (134 J K^{-1} mol^{-1}) and $\Delta G°$ (−367.01 J mol^{-1}) indicated that the adsorption process is endothermic and spontaneous with increasing disorder at the solid–solution interface.

Keywords Hydrothermal synthesis · Methyl Violet · Adsorption kinetic · Adsorption isotherm · Potassium aluminium fluoride phosphate

Introduction

Industrial discharges containing toxic products of organic nature such as dyes and pesticides or minerals such as heavy metals constitute the first source of the aquatic pollution. Their elimination represents one of the main problems in the treatment processes of liquid discharges. Dyes can be mutagenic and carcinogenic and can have harmful effects on the health such as dysfunction of kidney, reproductive system, liver, brain and central nervous system (Kadirvelu et al. 2003; Wang and You Hu 2007; Benzaquén et al. 2012). They can be classified as anionic (direct, acid and reactive dyes), cationic (basic dyes) and non-ionic (disperse dyes) (Mishra and Tripathy 1993). Due to their chemical aromatic structure, they are difficult to degrade biologically. Therefore, numerous physical and/or chemical methods were used for the removal of dyes like the electrochemistry (Giwa et al. 2019), coagulation (Morshedi et al. 2013), chemical oxidation (Nidheesh 2018), membranes (Khumalo et al. 2019), sono-electrochemistry (Radi et al. 2015), microbial (Liu et al. 2019) and Fenton process (Díez et al. 2018) and photocatalysis (Saidi et al. 2020; Fatimah et al. 2019; Chai et al. 2015; Dammala et al. 2019; Das et al. 2021). Among these methods, adsorption has been studied as one of the least expensive alternatives for wastewater treatment. It is therefore necessary to develop low-cost and available materials with high adsorption capacities. Nowadays a wide variety of adsorbents are used such as clay minerals (Park et al. 2019), chitin (Zazycki and Dotto 2019), membranes (Guo et al. 2018), natural phosphates, phosphates (Yan et al. 2019; Zhang et al. 2019), polymers (Yang et al. 2019), carbon (Lawal et al. 2019), nanoparticle (Uddin and Baig 2019).

✉ R. Bagtache
bagtacheradia@yahoo.fr

✉ M. Trari
mtrari@usthb.dz

[1] Laboratory of Electrochemistry-Corrosion, Metallurgy and Inorganic Chemistry, Faculty of Chemistry, (USTHB), BP 32, 16111 Algiers, Algeria

[2] Laboratory of Storage and Valorization of Renewable Energies, Faculty of Chemistry, (USTHB), BP 32, 16111 Algiers, Algeria

In this context, we report the synthesis and its physical characterization (XRD analysis, SEM microscopy, thermal gravimetry and diffuse reflectance) of potassium aluminum fluoride phosphate $KAlPO_4F$ that was further applied in the removal of methyl violet. It is worth noting that our synthesis differs slightly from those presented elsewhere, which require more time and expensive reagents (Kirkby et al. 1995a). To our knowledge, the literature reported only one article about application of $KAlPO_4F$ in the luminescence, activated by the rare earth Eu^{3+} (Akojwar et al. 2017). Isotherm, kinetic and thermodynamic models were used to fit the experimental adsorption data, in order to determine the adsorption characteristics and mechanisms.

Experimental

Synthesis

All reagents for the synthesis of our phosphate were obtained from commercial sources and used without any further purification. $KAlPO_4F$ was prepared by hydrothermal route; a mixture of $C_9H_{21}AlO_3$ (0.608 g, 97%); KOH (0.980 g); NaF (0.20 g) and distilled water (20 mL), was homogenized under magnetic stirring. The obtained gel was transferred into a Teflon-lined stainless steel autoclave and heated at 180 °C for 3 days under autogenously pressure. The white product was washed several times with distilled water and dried at 60 °C for 24 h.

Characterization

The X-ray diffraction (XRD) data were collected over the 2θ range (5–80°) with a Philips X'Pert Pro using Cu Kα radiation ($\lambda = 1.54056$ Å) at a scan rate of 2° (2θ) min^{-1}.

Diffuse Reflectance Spectrum was recorded with a Jasco 650 spectrophotometer using $BaSO_4$ as reference. The SEM image was taken with a JSM-6700F field-emission microscope operating at 5.0 kV. Thermal analysis (TG) was carried out under air flow over the range (20–600 °C) with a heating rate of 5 °C min^{-1}. The point of zero charge (pHpzc), an important controlling parameter in adsorption, was determined in $NaNO_3$ (0.1 M) solutions (25 mL) in which 25 mg of the adsorbent was added; the pH was adjusted in the region (2.0–10.0) using HCl and NaOH (0.01 M) solutions. The mixtures were stirred for 48 h and filtered; the pHs of the solutions were measured before contact (initial pH_i) and after filtration (final pH_f).

Adsorption

In this study, the methyl violet (MV, chemical formula $C_{25}H_{30}ClN_3$) was used as a pollutant dye. The stock MV solution (100 ppm) was diluted to the desired concentrations (10–60 ppm). Adsorption tests were performed as follows: The catalyst $KAlPO_4F$ (10 mg) was suspended in 10 mL of MV solution at room temperature (~20 °C) at natural pH (~7), not adjusted. When the contact the time was over, the mixture was centrifuged at 3000 rpm for 10 min. The remaining MV concentration was evaluated by measuring the absorbance at λ_{max} (= 582 nm). The adsorbed amount was calculated from the following expressions:

$$\text{Removal\%} = \frac{(C_o - C_e) \cdot 100}{C_o} \quad (1)$$

$$q_e = \left(\frac{V}{m}\right) \cdot (C_0 - C_e) \quad (2)$$

where C_o and C_e are the initial and equilibrium concentrations of MV (ppm), respectively, V the volume (L) of the solution, m (g) the adsorbentmass of $KAlPO_4F$ and q_e the amount of adsorbed MV (mg/g) at equilibrium.

Effect of initial pH

To study the pH influence on the adsorption capacity of the synthesized phosphate, experiments were performed at 20 °C with MV concentration of 10 ppm at different initial pHs 3, 5, 7.5 and 10. The pH of each solution was adjusted with HCl or NaOH (0.1 N).

Adsorption kinetic

The adsorption kinetic was studied by testing three theoretical models:

The pseudo-first-order

The pseudo-first-order kinetic is given by:

$$\frac{dq}{dt} = K_L(q_e - q_t) \quad (3)$$

where q_t is the adsorbed amount at time t (mg/g); q_e the adsorbed amount at equilibrium (mg/g) and K_L the rate constant (h^{-1}). After integration by applying the initial conditions, one obtains:

$$\ln\left(q_e - q_t\right) = \ln q_e - K_L t \quad (4)$$

The plot $\ln(q_e - q_t)$ against time (t) gives a straight line whose slope and intercept give, respectively, the rate constant k_L and $\ln q_e$.

Pseudo-second-order

The pseudo-second-order kinetic equation can be written in the following form:

$$\frac{dq_t}{dt} = K_2\left(q_2 - q_t\right)^2 \quad (5)$$

whose integration gives:

$$\frac{t}{q_t} = \frac{1}{K_2 q_e^2} + \frac{1}{q_e}t \quad (6)$$

The second-order rate constant K_2 (g mg^{-1} h^{-1}) is determined from the intercept of the linearized form of the pseudo-second-order equation.

Elovich model

This model, useful for describing the chemisorption, is expressed as follows:

$$q_t = \left(\frac{1}{b}\right)\ln(ab) + \frac{1}{b}\ln t \quad (7)$$

where a is the initial adsorption rate (mg/g min) and b the desorption constant related to the extent of surface coverage and activation energy (g/mg). The parameters (1/b) and (1/b) ln (ab) are deducted from Eq. 7.

Intraparticle diffusion model

The intraparticle diffusion model with multi-linearity, representing the different stages of adsorption, is given by:

$$q_t = K_p\sqrt{t} + c \quad (8)$$

where K_p is the diffusion coefficient and q_t is adsorbed amount. The plot q_t versus $\sqrt{t}$should be linear, with K_p as the slope and C as the intercept. Generally, a process is diffusion controlled if its rate depends on the rate at which the components diffuse to each other. A diffusion-controlled reaction should have a small activation energy (E_a), if E_a is large, then the reaction is not controlled by the diffusion rate but rather by the number of molecules whose energy is greater than E_a. The adsorption mechanism from the solution consists of three stages: (a) diffusion across the particle boundary layer, a process measured by an external device mass transfer coefficient; (b) diffusion within the solid; and (c) adsorption on the sites. Steps (a) and (b) are the major rate-controlling processes, while step (c) is assumed to be fast. It is proposed that two factors, primarily fluid velocity, can distinguish the diffusion-controlled systems from the chemically controlled systems.

Thermodynamic parameters

The standard free enthalpy ($\Delta G°$), standard enthalpy ($\Delta H°$) and standard entropy ($\Delta S°$) for the MV adsorption are also calculated. The knowledge of $\Delta G°$ predicts the spontaneity of the adsorption process, while the entropy $\Delta S°$ describes the degree of disorder or randomness of a system. As for $\Delta H°$, its determination is useful to know whether the process is exothermic or endothermic. $\Delta G°$ is calculated from the equilibrium constant (K):

$$\Delta G^{\circ} = -RT\ln K \quad (9)$$

R is the universal gas constant and T the absolute temperature.

$$K = \frac{C_s}{C_e} \quad (10)$$

where C_s is the amount of dye adsorbed on the adsorbent (mg/L).

The thermodynamic parameters $\Delta G°$, $\Delta H°$ and $\Delta S°$ are determined at different temperatures (293, 303 and 313 K), keeping all other operating parameters constant. The experimental results were used for the determination of thermodynamics:

$$\ln K = -\frac{\Delta G°}{RT} = \left(\frac{\Delta S°}{R}\right) - \left(\frac{\Delta H°}{RT}\right) \quad (11)$$

$\Delta H°$ and $\Delta S°$ are calculated from the slope and intercept of the plot ln K versus $1/T$.

Adsorption isotherms

The Freundlich, Langmuir, Temkin and Elovich models are commonly used to describe how the adsorbate interacts with the adsorbent and to understand the interaction mechanism. They also provide information on the surface properties of the adsorbent and its affinity with the adsorbate.

Freundlich model

In this model, the adsorption takes place on a heterogeneous surface, through a multilayer adsorption mechanism. The adsorbed amount at equilibrium (q_e) is related to the concentration (C_e) by the relation:

$$q_e = K_F \cdot C_e^{1/n} \quad (12)$$

where K_F is a constant related to the adsorption capacity of the adsorbent and 1/n its intensity. The linear form of the model is expressed as follows:

$$\ln q_e = \ln K_F + \frac{1}{n} \ln C_e \tag{13}$$

The values of K_F and $1/n$ are calculated from the intercept and slope of the straight-line plot of ln q_e versus ln C_e, respectively.

Langmuir model

Initially, this model described the adsorption of gas molecules onto metal surfaces and has been extended later to the sorption of various molecules and /or ions in liquid phase, onto different adsorbents. It is based on the assumption that the adsorption occurs on specific homogeneous sites on the adsorbent surface. Once a molecule occupies a site, no further adsorption can take place, leading to a monolayer adsorption:

$$q_e = \frac{q_m K_L C_e}{1 + K_L C_e} \tag{14}$$

where q_m is the maximum adsorption capacity (mg/g) and K_L a constant related to the adsorption energy (L/mg). The linearized form is as follows:

$$\frac{1}{q_e} = \left(\frac{1}{q_m}\right) + \left(\frac{1}{K_L \cdot C_e \cdot q_m}\right) \tag{15}$$

The essential characteristics of a Langmuir isotherm can be expressed in terms of a dimensionless separation factor or equilibrium parameter R_L, defined by Guiza (2017):

$$R_L = 1/\left(1 + K_L C_o\right) \tag{16}$$

The values of q_m and K_L were determined from the slope and intercept of the linear plot of $1/q_e$ versus $1/C_e$.

Elovich model

This relation differs from the previous model in the evolution of the adsorption site overlap: The number of available sites varies exponentially during adsorption, which implies adsorption in several layers:

$$\ln\left(\frac{q_e}{C_e}\right) = \ln\left(K_E \cdot q_{max}\right) - \left(\frac{q_e}{q_{max}}\right) \tag{17}$$

where C_e is the equilibrium concentration (mg/L), q_e the amount of product adsorbed per mass unit of the adsorbent (mg/g), q_{max} the theoretical maximum adsorption capacity (mg/g) and K_E the Elovich thermodynamic equilibrium constant (L/mg).

Temkin model

The isotherm is described by the following equation:

$$q_e = B\text{Ln}\, A_T + B\text{Ln}C_e \tag{18}$$

where $B = RT/\ b_T$ and B is a constant related to the heat of adsorption (J/mol), b_T and A_T are the isotherm constants (L/g).

Results and discussion

Characterization of the adsorbent

The XRD pattern of $KAlPO_4F$ prepared by hydrothermal route is shown in Fig. 1. The narrow peaks indicate a good crystallization, and they are indexed in an orthorhombic system with the space group Pnna. The lattice parameters: $a = 12.612(5)$, $b = 10.172(3)$, $c = 6.205$ Å are in a good agreement with those reported elsewhere (Kirkby et al. 1995b).

The SEM micrograph, illustrated in Fig. 2a, shows crystals with hexagonal sections. The structure is made up of AlF_2O_4 octahedra and PO_4 tetrahedra where the K^+ ions are disordered (Fig. 2b); a detailed description of the structure was previously reported (Kirkby et al. 1995b).

Thermal analysis shows that our phosphate is thermally stable up to 300 °C (Fig. 3). With raising temperature, a progressive weight loss occurs, accompanied by an exothermic peak, due to the decomposition of $KAlPO_4F$.

The UV–Vis adsorption spectrum of as-prepared material is shown in Fig. 4 (https://www.sciencedirect.com/science/article/abs/pii/S0277538717300736#f0030). The

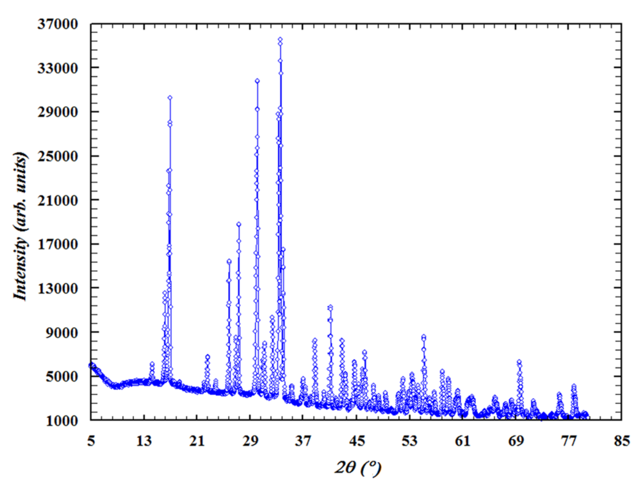

Fig. 1 X-ray diffraction pattern of $KAlPO_4F$ prepared by hydrothermal route

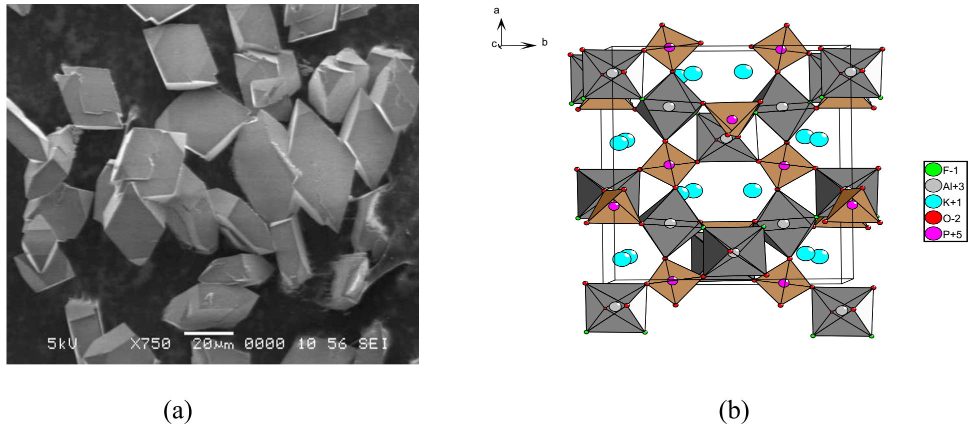

Fig. 2 **a** SEM of $KAlPO_4F$, **b** projection of the crystal structure of $KAlPO_4F$ along [001] axis

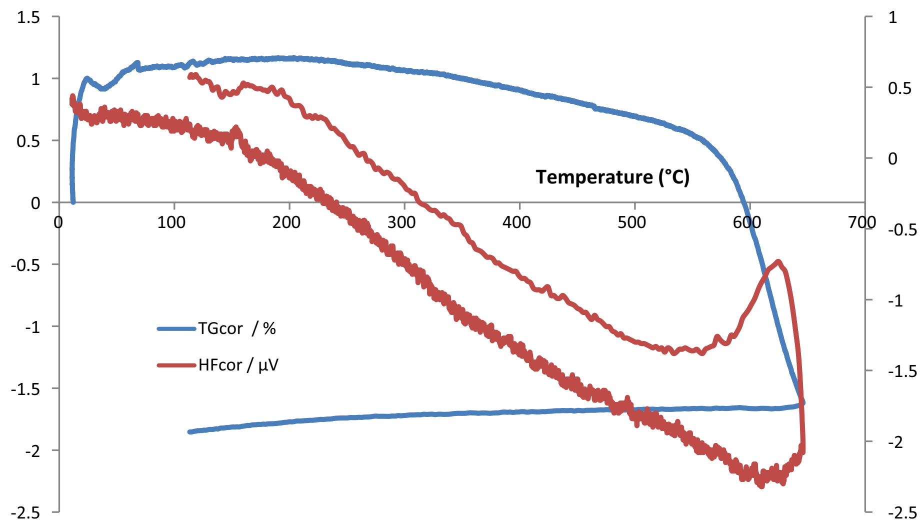

Fig. 3 Thermal analysis of $KAlPO_4F$ carried out under air flow at a heating rate of 5 °C min^{-1}

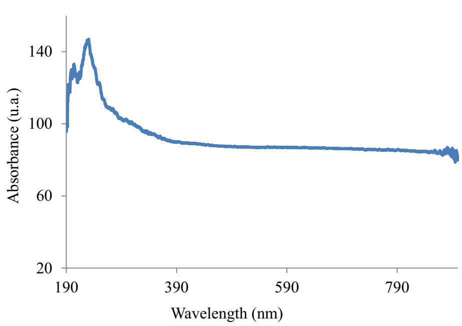

Fig. 4 UV–Visible diffuse reflectance of $KAlPO_4F$ synthetized hydrothermally at 180 °C

absorbance peaks 232 nm and decreases progressively to ~400 nm with a saturation up the near infrared. The bands at 218 and 232 nm correspond to oxygen to metal charge transfer transitions (Li et al. 2010).

The pHpzc was found to be 6.9 and corresponds to the point where the curve pH_f versus pH_i intersects the line $pH_f = pH_i$ (SM 1). This indicates a negative surface charge of the adsorbent at pH > 6.9, which becomes positive above pH 6.9. In our study, the pH of our solutions is ~7, close to the natural environment without any adjustment, so the surface of the compound is near neutrality. As expected, below pHpzc the surface inhibits the adsorption of MV, a cationic dye due to repulsive interactions of positive charges.

Adsorption studies

Effect of contact time

The effect of contact time on the MV adsorption was studied at 20 °C, in 10 mL MV solution (10 ppm) and adsorbent mass of 10 mg. The amount of adsorbed MV increases and slows down as the adsorption proceeds with increasing contact time and reaches equilibrium (Fig. 5a). The deceleration of the adsorption rate is reflected by a low increase in the uptake capacity of $KAlPO_4F$ due to the decrease in the MV amount in solution and the number of available binding sites

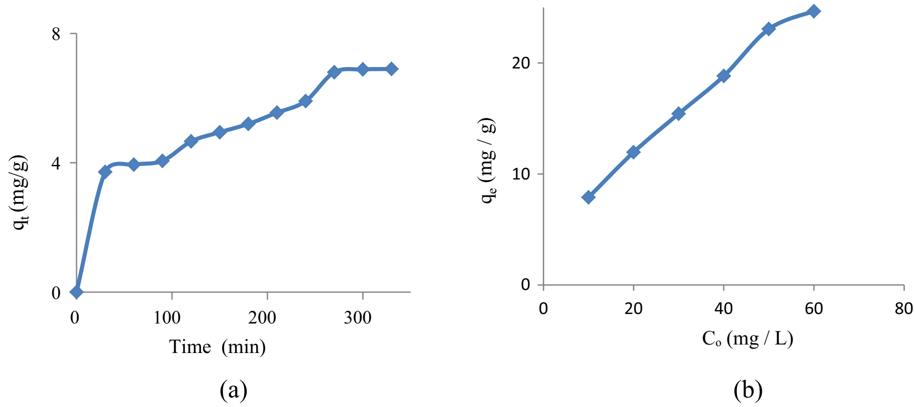

Fig. 5 **a** Effect of contact time on the MV adsorption onto $KAlPO_4F$, **b** effect of the initial concentration of MV solution

for adsorption; this stage lasts approximately ~50 min. The observed saturation up to 270 min is due to the almost total occupation of the adsorption sites.

Effect of initial dye concentration

The dyes in the real effluents reach concentrations as high as 40 ppm, and it is interesting to study the influence of this parameter on the MV adsorption. The initial dye concentration (C_o) is a critical parameter affecting the adsorption in wastewater treatment; its effect is shown in Fig. 5b (https://www.sciencedirect.com/science/article/abs/pii/S0277538717300736#f0060). The adsorption amount increases from 7 mg/g (at the lower MV initial concentration of 10 ppm) to 25 mg/g for concentration of C_o of 60 ppm. The increased adsorbed amount at equilibrium (mg/g) augments with the initial concentration C_o due to the increase of the driving force. The latter comes from the concentration gradient for the mass transfer with increasing C_o. In addition, it has been observed that the adsorption was rapid at the beginning due to the large number of vacant sites and gradually decreases as the adsorption proceeds until equilibrium. Over time, the remaining binding sites become difficult to reach because of the repulsive interactions between the MV species and the bulk phase.

Effect of initial pH

The pH effect on the MV removal was studied at different pHs (3, 5, 7.5 and 10) as shown in Fig. 6a under the working conditions (C_o = 10 ppm, T = 20 °C, catalyst dose 1 mg/mL). The results revealed an optimal adsorption at pH ~ 10 where the adsorption increases significantly due to attractive interactions between the cationic dye MV and the catalyst surface charged negatively. The high ionic strength leading to the attachment of MV molecules also accounts for the uptake performance on the vacant sites.

Effect of temperature

The adsorption studies were carried out at three different temperatures, namely 293, 303 and 313 K. The results showed that the adsorption percentage increased with increasing temperature, highlighting the endothermic nature of the removal process (Fig. 6b). This shows the affinity of binding sites for the MV molecules, which increases at high temperatures.

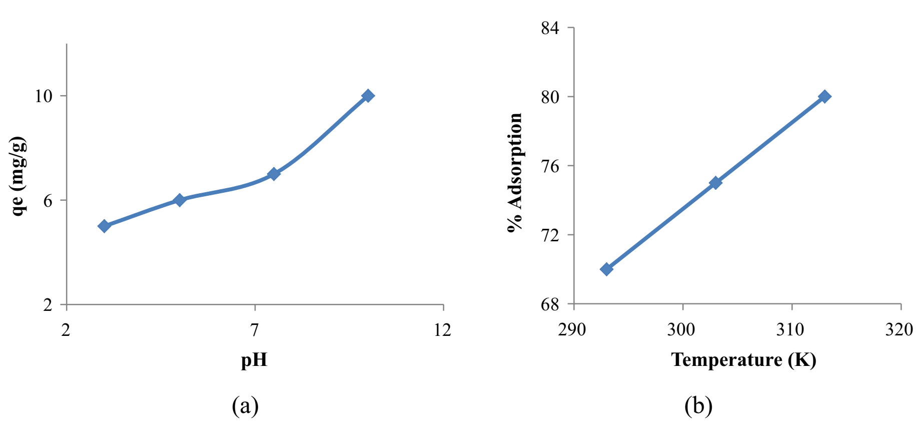

Fig. 6 **a** Effect of pH on the MV adsorption, **b** effect of temperature on the MV adsorption on $KAlPO_4F$

Kinetic modeling of MV adsorption

In the aim to elucidate the adsorption mechanism and rate-limiting steps, the pseudo-first-order, pseudo-second-order, Elovich and intraparticle models were used to fit the experimental data (Figs. 7a, b and 8a). The best kinetic model may be checked by the linear regression coefficient (R^2).

The R^2 value for the pseudo-second-order model is higher than that of the other models (Table 1), which indicates a better fitness. Moreover, the q_e value was found to be 8. 17 mg/g which is close to the experimental value. Generally, the bulk diffusion is assumed rapid and is not rate determining since the pseudo-second-order cannot elucidate the diffusion mechanism and the film diffusion is not negligible.

In the intraparticle model, the plot does not pass by the origin (Fig. 8b) and this indicates that the intraparticle diffusion is not the only rate-limiting step; other processes may be involved in the MV adsorption on $KAlPO_4F$.

The adsorption tends to be divided into two stages. The initial phase is generally referred to external mass transport and the next to the penetration of the adsorbate into the pores until equilibrium is reached; all parameters are listed in Table 2.

The intercept gives an idea about the thickness of the boundary layer, i.e., the larger intercept the greater is the boundary layer effect. The k_p values were calculated by using correlation analysis. The R^2 coefficients suggest that the MV uptake varies almost linearly with $t^{1/2}$. This

Fig. 7 **a** Pseudo-first-order, **b** pseudo-second-order kinetic model for the MV adsorption onto $KAlPO_4F$

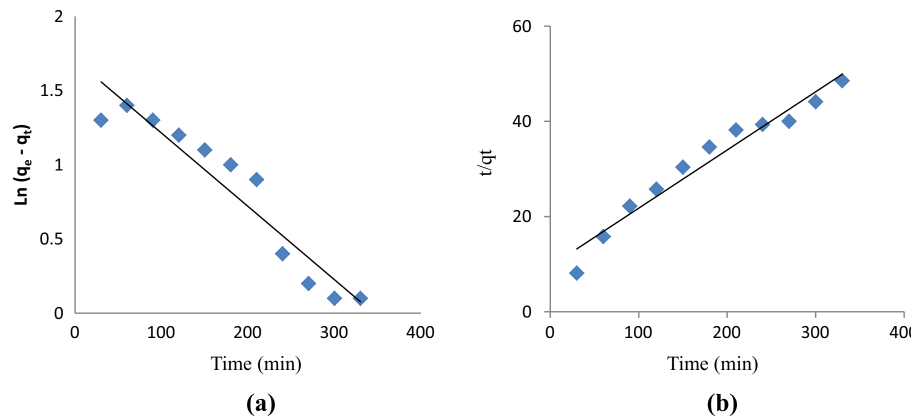

Fig. 8 **a** Elovich kinetic, **b** intra-particle kinetic models for the MV adsorption onto $KAlPO_4F$

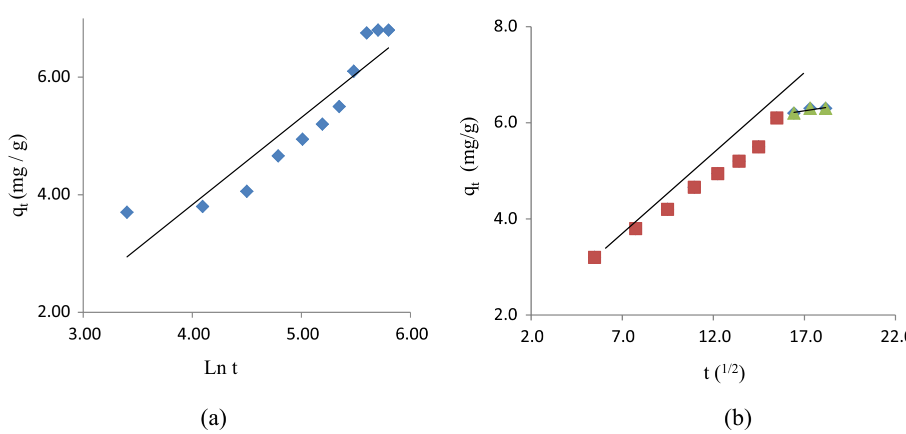

Table 1 Adsorption kinetic parameters for the MV adsorption on $KAlPO_4F$ for the pseudo-first-order, pseudo-second-order and Elovich models at 293 K

Pseudo-first-order model	Pseudo-second-order model					Elovich model		
K_1 (min^{-1})	R^2	q_e (mg/g)	K_2 (g/mg min)	R^2	q_e (mg/g)	R^2	b	a
0.005	0.90	5.51	0.002	0.95	8.17	0.86	0.68	0.36

Table 2 Kinetic parameters for intraparticle diffusion model for the MV adsorption (10 mg/L) on $KAlPO_4F$, at 293 K

1st line			2nd line		
K_{p1} (mmol/g min$^{1/2}$)	R^2	C (mmol/g)	K_{p2} (mmol/g min$^{1/2}$)	R^2	C (mmol/g)
0.27	0.99	1.66	0.03	0.76	6.28

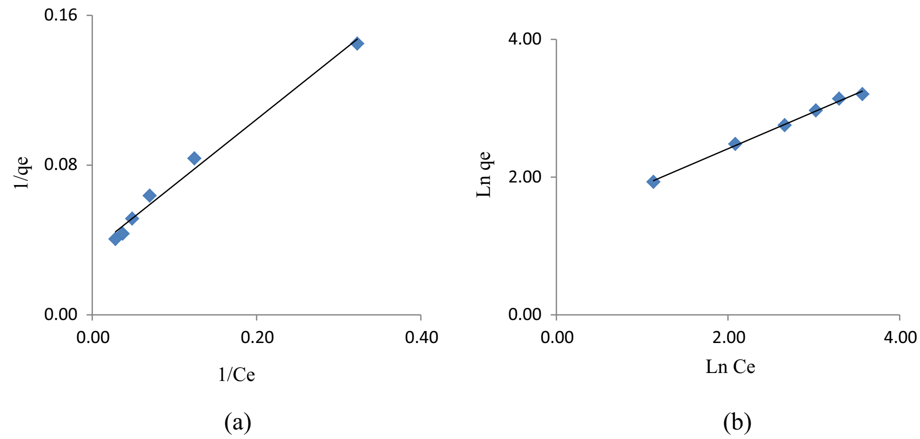

Fig. 9 **a** Langmuir model, **b** Freundlich models for the MV adsorption onto $KAlPO_4F$

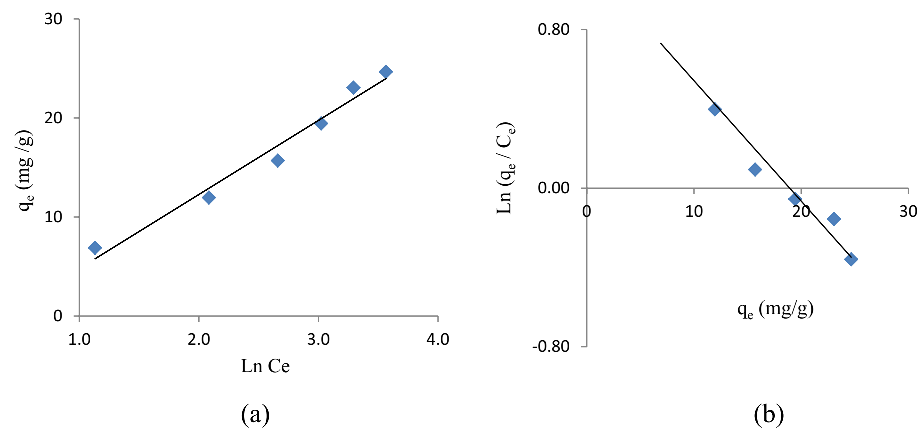

Fig. 10 **a** Elovich, **b** Temkin kinetic models for the MV adsorption onto $KAlPO_4F$

Table 3 Summary of isotherm parameters by using Langmuir, Freundlich, Elovich and Temkin models for MV adsorption (10 mg/L) on $KAlPO_4F$, at 293 K

Model	Parameters			
Langmuir	R^2 0.98	K_L (L mg^{-1}) 0.09	q_m (mg g^{-1}) 29.41	R_L (L mg^{-1}) 0.52
Freundlich	R^2 0.99	K_F (L g^{-1}) 3.84	n_F 1.87	
Elovich	R^2 0.97	K_E (L mol^{-1}) 0.19	q_m (mg g^{-1}) 16.47	
Temkin	R^2 0.97	A_T (L g^{-1}) 1.43	B (J mol^{-1}) 7.47	b_T 326.13

functional relationship corresponds to the characteristic of the intraparticle diffusion.

Adsorption isotherms

The various isotherm models are presented in Figs. 9a, b and 10a, b, and the constants values are summarized in Table 3. According to the regression coefficients R^2, the Freundlich isotherm seems to be the best to describe the adsorption data, suggesting that MV molecules are adsorbed on several binding sites. The value of n is higher than 1 ($n = 1.87$), and this indicates a favorable adsorption of MV onto $KAlPO_4F$.

Adsorption thermodynamics

The thermodynamic functions give in-depth information of energetic exchanges association the adsorption process and are reliably determined. The adsorption capacity of

MV onto $KAlPO_4F$ increases with raising temperature in the range (293–313 K), beyond which the loss by vaporization becomes problematic. The insights of the adsorption mechanism are determined from the thermodynamic standard parameters, namely the enthalpy (ΔH°), entropy (ΔS°) and free enthalpy (ΔG°).

The positive enthalpy ΔH° and negative free enthalpy ΔG° show an endothermic and spontaneous MV adsorption (Table 4) (https://www.sciencedirect.com/science/article/pii/S221237171400016X#t0040). The low ΔH° value (<40 kJ/mol) suggested that the uptake mechanism is typically considered to be that of physisorption bonds (Kirkby et al. 1995a, 1995b; Akojwar et al. 2017; Guiza 2017; Li et al. 2010; Bello et al. 2012); the chemisorption interactions are between 80 and 420 kJ/mol. In other words, the positive enthalpy ΔH° indicates that the adsorption of MV molecules onto $KAlPO_4F$ is endothermic corroborated by the increased adsorbed amount as temperature increases.

The positive entropy ΔS° shows that the degree of freedom increases at the solid–liquid junction during the MV adsorption.

The equilibrium constant (K) was calculated from the amount of dye adsorbed on the adsorbent (mg/L). ΔH° and ΔS° are deduced from the slope and intercept of the linear plot ln K versus $1/T$ (Fig. 11). A more negative ΔG° signifies a great driving force of adsorption, resulting in increased adsorption capacity.

Table 5 gives the adsorption capacity of our material compared with those reported in the literature (Mall et al. 2006; Ofomaja and Ho 2008; Ahmad 2009; Rahchamani et al. 2011; Sama Al-Jubouri et al. 2023; Ali Nisreen et al. 2022; Kashif Uddin et al. 2021; Hadj-Otmane et al. 2020; Kua et al. 2020; Xiang et al. 2024) and shows that our synthetized $KAlPO_4F$ possesses relatively a good adsorption.

The hydrothermally developed $KAlPO_4F$ adsorbent has proven to be suitable for the removal of dyes from aqueous solutions, due to its availability, low-cost preparation and good adsorption capacity.

Table 4 Thermodynamic parameters for MV dye adsorption onto $KAlPO_4F$

T (°C)	ΔS° ($J\ K^{-1}\ mol^{-1}$)	ΔH° ($J\ mol^{-1}$)	R^2	ΔG° ($J\ mol^{-1}$)
Parameters				
20	134	39034	0.99	−367.01
30				−1632.52
40				−2971.83

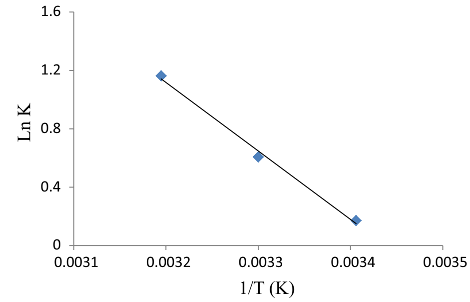

Fig. 11 Ln K versus $1/T$ for the MV adsorption on $KAlPO_4F$

Conclusion

$KAlPO_4F$ was synthesized hydrothermally at 453 K, a time-consuming method using inexpensive reagents. The present study showed that $KAlPO_4F$ is relatively a potential adsorbent for the removal of crystal violet dye from aqueous solutions. The results indicated that the experimental kinetic data fitted best the pseudo-second-order model with a multi-step diffusion. The adsorption process was well described by the Freundlich model, and the equilibrium time was reached within 270 min at 20 °C. The thermodynamic parameters were also calculated, and the positive enthalpy ΔH° indicates that the MV adsorption was endothermic and spontaneous. The effect of the initial concentration of the solute on the rate of reaction was significant. The uptake rate of methyl violet increased with increasing the initial concentration, temperature and pH. Moreover, the best result was observed at pH 10 and the equilibrium was reached within 270 min.

Supplementary Information The online version contains supplementary material available at https://doi.org/10.1007/s13201-024-02116-3.

Table 5 Comparison of reported adsorption capacities of MV for adsorbents

Adsorbent	Q_{max} (mg/g)	References
Bagasse fly ash	26.25	Mall et al. (2006)
Mansonia wood sawdust	24.6	Ofomaja and Ho (2008)
CPBP	32.78	Ahmad (2009)
PAA	1136	Rahchamani et al. (2011)
Zeolite nanocrystals composite (NYC)	108.7	Sama Al-Jubouri et al. (2023)
Date seeds	59.9	Ali Nisreen et al. (2022)
M-MoS_2@bentoniteNC	384.61	Kashif Uddin et al. (2021)
DPP-biochar	18.8	Hadj-Otmane et al. (2020)
Ipomoea aquatica (IA)	267.9	Kua et al. (2020)
Bio-MOF-2Me	157.1	Xiang et al. (2024)
$KAlPO_4F$	29.41	This work

Acknowledgements The authors would like to thank the Faculty of Chemistry (Algiers) for providing the financial support of this work.

Funding The author(s) received no specific funding for this work.

Declarations

Conflict of interest The authors attest that there are not conflict of interest financial, personal or other relationships with other people, laboratories or organizations worldwide.

References

Ahmad R (2009) Studies on adsorption of crystal violet dye from aqueous solution onto coniferous pinus bark powder (CPBP). J Hazard Mater 171:767–773

Akojwar A, Shinde KN, Kokode NS (2017) Orange-red luminescence in $KAl_{1-x} PO_4$ F: Eu_x^{3+} ($0.1 \le x \le 1.0$) halophosphate phosphor by a novel facile combustion method. Res Phys 7:1161–1166

Ali Nisreen S, Jabbar NM, Alardhi SM, Majdi HS, Albayati TM (2022) Adsorption of methyl violet dye onto a prepared bio-adsorbent from date seeds: isotherm, kinetics, and thermodynamic studies. Heliyon 8:10276

Al-Jubouri SM, Al-Jendeel HA, Rashid SA, Al-Batty S (2023) Green synthesis of porous carbon cross-linked Y zeolite nanocrystals material and its performance for adsorptive removal of a methyl violet dye from water. Microporous Mesoporous Mater 356:112587

Bello OS, Fatona TA, Falaye FS, Osuolale OM, Njoku VO (2012) Adsorption of eosin dye from aqueous solution using groundnut hull–based activated carbon: kinetic, equilibrium, and thermodynamic studies. Environ Eng Sci 29:186–194

Benzaquén TB, Benzzo MT, Isla MA, Alfano OM (2012) Impact of some herbicides on the biomass activity in biological treatment plants and biodegradability enhancement by a photo-Fenton process. Water Sci Technol 67:210–216

Chai Y, Ding J, Wang L, Liu Q, Ren J, Dai WL (2015) Enormous enhancement in photocatalytic performance of Ag_3PO_4/HAp composite: a Z-scheme mechanism insight. Appl Catal B 179:29–36

Dammala P, Machado J, Rani B, Murali S, Devi S, Luwang MN, Sahu NK (2019) Synthesis of biphasic nanomaterials based on ZnO and SnO_2: application towards photocatalytic degradation of acid red dye. Nano Struct Nano Objects 18:100292

Das KC, Dhar SS, Thakurata DG, Das J (2021) Sn(II) inserted on hydroxyapatite encapsulated nickel ferrite ($NiFe_2O_4$@ HAp-Sn^{2+}): a novel nanocomposite for the effective photo-degradation of rhodamine B dye. J Clean Prod 290:125172

Díez AM, Sanromán MA, Pazos M (2018) Fenton-based processes for the regeneration of catalytic adsorbents. Catal Today 313:122–127

Fatimah I, Fahrani D, Harmawantika T, Sahroni I, Kamari A, A'bana Rahmatillah C, Nurillahi R (2019) Functionalization of hydroxyapatite derived from cockle (Anadara granosa) shells into hydroxyapatite–nano TiO_2 for photocatalytic degradation of methyl violet. Sustain Environ Res 40:29

Giwa A, Dindi A, Kujawa J (2019) Membrane bioreactors and electrochemical processes for treatment of wastewaters containing heavy metal ions, organics, micropollutants and dyes: recent developments. J Hazard Mater 370:172–195

Guiza S (2017) Biosorption of heavy metal from aqueous solution using cellulosic waste orange peel. Ecol Eng 99:134–140

Guo A, Ban Y, Yang K, Yang W (2018) Metal-organic framework-based mixed matrix membranes: Synergetic effect of adsorption and diffusion for CO_2/CH_4 separation. J Membr Sci 562:76–84

Hadj-Otmane C, Ouakouak A, Youcef L, Nguyen TH (2020) One-stage preparation of palm petiole-derived biochar: characterization and application for adsorption of crystal violet dye in water. Environ Technol Innov 19:100872

Kadirvelu K, Kavipriya M, Kathika C, Radhika M, Vennilamani N, Pattabhi S (2003) Utilization of various agricultural wastes for activated carbon preparation and application for the removal of dyes and metal ions from aqueous solutions. Bioresour Technol 87:129–132

Khumalo NP, Nthunya LN, De Canck E, Derese S, Verliefde AR, Kuvarega AT, Mamba BB, Mhlanga SD, Dlamini DS (2019) Congo red dye removal by direct membrane distillation using PVDF/PTFE membrane. Sep Purif Technol 211:578–586

Kirkby SJ, Lough AJ, Ozin GA (1995b) Crystal structure of potassium aluminium fluoride phosphate $KAlFPO_4$. Zeitschrift Für Kristallographie - Cryst Mater 12:210

Kua TL, Kooh MRR, Dahri MK, Zaidi NAHM, Lu YC, Lim LBL (2020) Aquatic plant, Ipomoea aquatica, as a potential low-cost adsorbent for the effective removal of toxic methyl violet 2B dye. Appl Water Sci 10:243

Lawal IA, Lawal MM, Azeez MA, Ndungu P (2019) Theoretical and experimental adsorption studies of phenol and crystal violet dye on carbon nanotube functionalized with deep eutectic solvent. J Mol Liq 288:110895

Li Y-F, Hubble DG, Miller RG, Zhao H-Y, Pan W-P, Parkin S, Yan B (2010) Synthesis and characterization of two novel organic–inorganic hybrid solids from Keggin ions and metal coordination complexes. Polyhedron 29:3324–3328

Liu J, Chen F, Li C, Lu L, Hu C, Wei Y, Raymer P, Huang Q (2019) Characterization and utilization of industrial microbial waste as novel adsorbent to remove single and mixed dyes from water. J Clean Prod 208:552–562

Mall ID, Srivastava VC, Agarwal NK (2006) Removal of orange-G and methyl violet dyes by adsorption onto bagasse fly ash-kinetic study and equilibrium isotherm analyses. Dyes Pigm 69:210–223

Mishra G, Tripathy M (1993) A critical review of the treatments for decolourization of textile effluent. Colourage 40:35–38

Morshedi D, Mohammadi Z, Mashhadi M, Boojar A, Aliakbari F (2013) Using protein nanofibrils to remove azo dyes from aqueous solution by the coagulation process. Colloids Surf B Biointerfaces 112:245–254

Nidheesh PV, Zhou M, Oturan MA (2018) An overview on the removal of synthetic dyes from water by electrochemical advanced oxidation processes. Chemosphere 197:210–227

Ofomaja AE, Ho YS (2008) Effect of temperatures and pH on Methyl Violet biosorption by Mansonia wood sawdust. Bioresour Technol 99:5411–5417

Park SM, Lee J, Jeon EK, Kang S, Alam MS, Tsang DCW, Alessi DS, Baek K (2019) Adsorption characteristics of cesium on the clay minerals: Structural change under wetting and drying condition. Geoderma 340:49–54

Radi MA, Nasirizadeh N, Moghadam MR, Dehghani M (2015) The comparison of sonochemistry, electrochemistry and sonoelectrochemistry techniques on decolorization of C.I reactive blue 49. Ultrason Sonochemistry 27:609–615

Rahchamani J, Mousavi HZ, Behzad M (2011) Adsorption of methyl violet from aqueous solution by polyacrylamide as an adsorbent: Isotherm and kinetic studies. Desalination 267:256–260

Saidi M, Benomara A, Mokhtari M, Boukli-Hacene L (2020) Sonochemical synthesis of Zr-fumaric based metal-organic framework (MOF) and its performance evaluation in methyl violet 2B decolorization by photocatalysis. React Kinet Mech Cat 131:1009–1021

Uddin MK, Baig U (2019) Synthesis of Co_3O_4 nanoparticles and their performance towards methyl orange dye removal: characterisation, adsorption and response surface methodology. J Clean Prod 211:1141–1153

Uddin MK, Mashkoor F, AlArifi IM, Nasar A (2021) Simple one-step synthesis process of novel MoS_2@bentonite magnetic nanocomposite for efficient adsorption of crystal violet from aqueous solution. Mater Res Bull 139:111279

Wang BE, You Hu Y (2007) Comparison of four supports for adsorption of reactive dyes by immobilized Aspergillus fumigatus beads. J Environ Sci 19:451–457

Xiang W, Wang Q, Li Z, Dong J, Liu J, Zhang L, Xia T, He Y, Zhao D (2024) Water-stable methyl-modified MOF and mixed matrix membrane for efficient adsorption and separation of cationic dyes. Sep Purif Technol 330:125268

Yan JC, Ren J, Ren LL, Jian JM, Yang Y, Yang SF, Ren TL (2019) Development of a portable setup using a miniaturized and high precision colorimeter for the estimation of phosphate in natural water. Anal Chim Acta. https://doi.org/10.1016/j.aca.2019.01.030

Yang X, Yang QH, Fu Y, Wu F, Huang JH, Luo MB (2019) Study on the adsorption process of a semi-flexible polymer onto homogeneous attractive surfaces. Polymer 172:83–90

Zazycki MA, Dotto GL (2019) Chitin derived biochar as an alternative adsorbent to treat colored effluents containing methyl violet dye. Adv Powder Technol 30:1494–1503

Zhang H, Elskens M, Chen G, Chou L (2019) Phosphate adsorption on hydrous ferric oxide (HFO) at different salinities and pHs. Chemosphere 225:352–359